Control Engineering Practice 145 (2024) 105878

Contents lists available at ScienceDirect

Control Engineering Practice

journal homepage: www.elsevier.com/locate/conengprac

Parameterised function ILC with application to stroke rehabilitation

Xiaoru Sun *, Chris T. Freeman

School of Electronics and Computer Science, University of Southampton, University Road, Southampton, SO17 1BJ, Hampshire, UK

ARTICLE INFO

Keywords:
Iterative learning control
Functional electrical stimulation
Stroke rehabilitation
Assistive technology

ABSTRACT

Functional electrical stimulation (FES) is a popular assistive technology that uses electrical impulses to artificially stimulate muscles to help paralysed or impaired subjects regain their lost movement after stroke. A large number of FES elements can be combined to form FES arrays which are capable of activating the multiple muscles needed to perform functional arm movements. However, the control of FES arrays is challenging since high precision is required but there is little time available in a clinical or home setting to identify a model. To date, by far the highest accuracy has been achieved using iterative learning control (ILC), a technique that mirrors the repeated nature of rehabilitation task practice. In particular, high accuracy has been achieved using a well-known ILC law for a general class of nonlinear systems which computes the updated control input using a linearised plant model. Since a global system model is unavailable, this is identified on every ILC trial by running an identification test. This adds many time-consuming identification tests, making it infeasible for clinical deployment.

To solve this problem, an approach is developed that can deliver high accuracy with minimal identification overhead. It introduces a parameterised plant model that is updated in parallel with the ILC using all available data, and then applied to replace identification tests. Rigorous conditions are derived to ensure convergence is preserved while minimising identification time. Numerical results show that four references can be tracked using only 10.8% of the experimental tests required by standard ILC algorithms. The approach is then applied experimentally to six unimpaired subjects using a realistic rehabilitation scenario. In particular, a novel stereo camera system is used to measure hand joint angles in a manner that can transfer to home use. Results show mean joint angle tracking accuracy within 5°, while requiring only between 25% and 64.9% of the experimental tests of standard ILC.

1. Introduction

Every year 13.7 million people worldwide suffer from stroke (Feigin et al., 2022). Approximately 40% of stroke survivors are left permanently disabled or paralysed, making stroke the leading cause of adult disability (Hankey, 2017). Conventional therapy is increasingly expensive and difficult to obtain. It also provides only limited recovery and there is increasing pressure to find low cost technologies that support sensorimotor recovery. FES artificially activates muscles by applying electrical impulses via implanted or surface electrodes, and is the most frequently used rehabilitative and assistive technology (Hughes et al., 2014). FES can either replace lost function or facilitate rehabilitation over repeated task practice, and in both cases the aim is to deliver precise functional movements that support the activities needed for daily living.

FES is strongly recommended by the recent UK National Clinical Guidelines for stroke (The Stroke Association, 2023) which have confirmed its potential to provide effective therapy for people with wrist and finger weakness following a stroke. The guidelines also highlight the fact that current systems tested in clinics and hospitals employ open-loop control that is neither personalised to user needs, nor geared towards achieving a functional task.

Another limitation of the commercial systems employed clinically is their use of large single pad electrodes. These are difficult to position and it takes significant time and practice to find the optimal electrode location (Bijelić, Popović-Bijelić, Jorgovanović, Bojanić, & Popović, 2004), even by experienced users. A more fundamental limitation is their selectivity. Sites for different muscles overlap, making selective stimulation with single electrodes impossible. To address both issues, electrode arrays have been developed and consist of multiple pads integrated on a flexible printed circuit board or within a textile. Prominent examples are Shefstim (Heller et al., 2013), INTFES (Velik, Malesevic, Maneski, Hoffmann, & Keller, 2011), RehaMovePro (Valtin et al., 2016), SMARTmove (Ward et al., 2020; Yang et al., 2018). These use grid layouts, while Crema et al. (2018), Molteni et al. (2018),

* Corresponding author.
E-mail address: sunxiaoru.yb@gmail.com (X. Sun).

https://doi.org/10.1016/j.conengprac.2024.105878
Received 18 September 2023; Received in revised form 29 January 2024; Accepted 30 January 2024
Available online 7 February 2024

Pedrocchi et al. (2013) locate the electrodes over specific forearm muscles. Although FES arrays can provide high resolution stimulation, the number of elements and the sensitivity in their positioning makes their control extremely challenging. This is amplified by the complexity of the musculoskeletal system to which they are attached. This issue has resulted in most FES controllers mimicking the way a therapist moves an electrode to find an optimum location for stimulation. A full review is given in Salchow-Hömmen, Pedrocchi, and Keller (2020) and is summarised next.

The first controllers for FES arrays involved manually selecting array elements based on visual assessment of the resulting movements (Bijelić et al., 2004). These then progressed to using sensor data to assess the joint angle deviation (O'Dwyer, O'Keeffe, Coote, & Lyons, 2006). Automatic procedures followed in which each array element was stimulated in turn to find the one producing most force (Keller, Hackl, Lawrence, & Kuhn, 2006; Popović & Popović, 2009; Schill, Rupp, Pylatiuk, Schulz, & Reischl, 2009), taking up to ten minutes. Later modifications used combinations of electrodes (Hoffmann, Deinhofer, & Keller, 2012), the muscle twitch response (Malešević et al., 2012), points specified by therapists (Popović-Maneski et al., 2013), and electromyography (Marchis, Monteiro, Simon-Martinez, Conforto, & Gharabaghi, 2016; Popović-Maneski et al., 2016) to reduce the search time. However, all these approaches are based on extensively testing the response of each array element, followed by open-loop control. They are therefore inaccurate and highly time-consuming.

No model-based controllers have yet been used, due to the difficulty in identifying the system which is nonlinear, has many inputs/outputs, and is highly sensitive to changes in placement. The exception is ILC, which exploits the repeated nature of rehabilitation training. ILC uses experimental input and output data from previous attempts at a tracking task, often with a plant model, to update the control input signal. Each attempt is termed a 'trial', and the aim is to sequentially reduce the tracking error as the number of trials increases. This exactly coincides with the repeated nature of rehabilitation in which patients practice the same movement in order to retrain their neural pathways. ILC has outperformed alternative approaches and is the only model-based upper limb approach to have been used in clinical trials for upper limb rehabilitation (Freeman, 2016). ILC was applied in Freeman (2014), Ward et al. (2020), Yang et al. (2018) to control wrist and hand gestures (24 element array, 12 joint angles), achieving a mean absolute joint angle error of less than 5°. The approach required three ILC trials, with each involving an identification procedure taking three minutes to find a local model of the dynamics needed to compute the next update. The overall set-up time was more than ten minutes, and had to be repeated for each new gesture. This is far too long for clinical or home use.

One other alternative has been proposed, in the form of a recurrent fuzzy artificial neural network. This was applied in Imatz.-Ojanguren, Irigoyen, and Keller (2016), Imatz.-Ojanguren, Irigoyen, Valencia-Blanco, and Keller (2016) to map the relationship between sixteen array elements and the resulting wrist/finger angles. The training data were randomised which is uncomfortable to patients, and only used one electrode at a time, so could not capture the nonlinear effects of multi-element stimulation. Data were also collected by an instrumented glove which is unsuitable for patients. Despite these limitations, experimental results with six able-bodied and neurologically impaired subjects showed accuracy over 60%. However, the need for training meant that the approach suffered from the previous limitation, requiring forty-five minutes to set up.

This paper addresses the problem that there are no model-based FES array controllers that are suitable for clinical deployment. It develops a new ILC approach that can deliver high accuracy with significantly fewer additional tests than existing standard ILC or data-driven ILC approaches, see Huo, Freeman, and Liu (2020) for a review. It can be used for a general class of nonlinear systems, which includes the FES array based motion control problem. The approach builds on the proven ILC methodology of Freeman (2014), but introduces a 'parameterised function' model that replaces inter-trial identification test by harnessing all previous system input–output data while maintaining accuracy. Convergence conditions are derived to minimise the identification time while guaranteeing convergence to minimal error. A numerical example shows that standard ILC requires 129 experimental tests, while the proposed approach only needs 30 experimental tests. The approach is then applied experimentally to six unimpaired subjects, using FES hardware that is suitable for clinical deployment. Initial results appeared in Sun and Freeman (2022) but did not include hardware development, implementation, or practical validation results. To summarise, the contributions of this paper are:

- Developing a framework that enables a common class of nonlinear ILC update to remove identification tests, thereby significantly improving deployment speed and practical utility,
- Deriving new convergence properties for the well-known gradient ILC update, and using them to provide a quantitative comparison with the new framework,
- Translating the convergence conditions into a practical design framework that enables the designer to transparently balance tracking accuracy with overall test time,
- Matching the highest accuracy to have been demonstrated in the literature in upper limb motion tests, while using only 10.8% of the experimental tests required by previous ILC schemes, and
- Demonstrating the first use of a stereo camera system to record upper limb wrist and hard gestures during real-time FES control.

These contributions are a critical step towards translating FES upper limb rehabilitation into patients' homes.

The paper is arranged as follows: the standard ILC problem is defined in Section 2, with detailed convergence conditions derived in Section 3. Section 4 introduces parameterised function ILC using an updated parameterised model to replace system identification tests. To verify effectiveness of the algorithm, simulation results follow in Section 5. Experimental results follow in Section 6, with conclusions set out in Section 7.

2. Problem description

Consider the standard nonlinear discrete ILC problem in which the system dynamics are given by

$$\begin{aligned} x_k(t+1) &= f\left(x_k(t), u_k(t)\right), \quad x_k(0) = x_0, \\ y_k(t) &= h\left(x_k(t)\right), \qquad t = 0, 1, \ldots, N \end{aligned} \tag{1}$$

with the state vector $x_k(t) \in \mathbb{R}^q$. Here $f(\cdot)$ and $h(\cdot)$ are continuously differentiable with respect to their arguments. This system has m inputs and p outputs, and at time instant t the input is denoted $u_k(t) \in \mathbb{R}^m$ and the output is denoted $y_k(t) \in \mathbb{R}^p$. The objective is for $y_k(t)$ to track a reference $r(t) \in \mathbb{R}^p$ over the time instants $t = 1, 2, \ldots, N$ where $N < \infty$ is the number of samples in each ILC trial. The system is assumed to undertake the same tracking task over repeated trials, denoted using subscript k, where $k = 0, 1, 2, \ldots$. The system is reset to identical initial conditions between each trial.

To match the needs of patients undergoing rehabilitation, it is assumed that a set of n references, $\mathcal{R} = \{r_1, r_2, \ldots, r_n\}$ must be tracked. In common with the standard ILC problem description, see for example Freeman (2014, 2016), Freeman, Rogers, Hughes, Burridge, and Meadmore (2012), Lin, Owens, and Hatonen (2006), Rogers, Chu, Freeman, and Lewin (2023), noise is not included in subsequent analysis but its effect will be examined experimentally.

To compactly represent the system, the next step is to introduce the super-vectors

$$\boldsymbol{u_k} = \begin{bmatrix} u_k(0)^\top, & u_k(1)^\top, & \ldots & u_k(N-1)^\top \end{bmatrix}^\top \in \mathbb{R}^{mN}, \tag{2}$$

$$\boldsymbol{y_k} = \begin{bmatrix} y_k(1)^\top, & y_k(2)^\top, & \ldots & y_k(N)^\top \end{bmatrix}^\top \in \mathbb{R}^{pN}, \tag{3}$$

$$\boldsymbol{r} = \left[\begin{array}{cccc} r(1)^\top, & r(2)^\top, & \dots & r(N)^\top \end{array}\right]^\top \in \mathbb{R}^{pN} \tag{4}$$

This enables the system (1) to be expressed as the vector mapping $\boldsymbol{y}_k = \boldsymbol{g}(\boldsymbol{u}_k) : \mathbb{R}^{mN} \to \mathbb{R}^{pN}$ where $\boldsymbol{g}(\boldsymbol{u}_k) = [g_1(\boldsymbol{u}_k)^\top, \dots\ g_N(\boldsymbol{u}_k)^\top]^\top$ with the $t = 1, \dots N$ elements

$$\begin{aligned} g_t(x_k(0), u_k(0), \dots u_k(t-1)) &= h(x_k(t)) \\ &= h(f(x_k(t-1), u_k(t-1))), \\ &= h(f(f(x_k(t-2), u_k(t-2)), u_k(t-1))), \\ &\quad\ \vdots \\ &= h(f(f(\cdots f(x_k(0), u_k(0)), \dots, u_k(t-2)), u_k(t-1))). \end{aligned}$$

The aim of the standard ILC problem is to track a single reference perfectly. The control objective considered in this paper extends the standard ILC aim of tracking only one reference, and also introduces an additional design goal of reducing the number of trials. Furthermore, it relaxes the assumption that perfect tracking is possible. It is summarised as:

Definition 1 (*ILC Multi-Reference Problem*). $\forall \boldsymbol{r}_i \in \mathcal{R}$ generate a sequence of inputs, $\{\boldsymbol{u}_k\}_{k=0,1,\dots}$ such that

$$\begin{aligned} &\lim_{k\to\infty} \left\|\boldsymbol{u}_i^* - \boldsymbol{u}_k\right\|^2 = 0, \quad \boldsymbol{u}_i^* := \arg\min_{\boldsymbol{u}} J_i(\boldsymbol{u}), \\ &\qquad J_i(\boldsymbol{u}) = \left\|\boldsymbol{r}_i - \boldsymbol{g}(\boldsymbol{u})\right\|^2 \end{aligned} \tag{5}$$

without knowledge of system dynamics (1) and using the minimum identification tests.

Denote $k_{i,\delta}$ as the minimum number of trials required to achieve the closest possible tracking of $\boldsymbol{r}_i$, i.e.

$$k_{i,\delta} := \min\{k : \left|J_i(\boldsymbol{u}_k) - J_i(\boldsymbol{u}^*)\right| < \delta\}. \tag{6}$$

where δ is a positive scalar. Then an additional aim is minimise the total number of trials, i.e.

$$\min k_\delta, \quad k_\delta := \sum_{i=1}^{n} k_{i,\delta} \tag{7}$$

needed to track all n references.

3. ILC application

Having defined the problem, this section introduces the ILC update form used in FES based rehabilitation (Freeman, 2014; Ward et al., 2020; Yang et al., 2018) and analyses its performance.

For one reference $\boldsymbol{r}_i$, the ILC objective can be solved using the standard update form

$$\boldsymbol{u}_{k+1} = \boldsymbol{u}_k + L(\boldsymbol{r}_i - \boldsymbol{y}_k) \tag{8}$$

where $\boldsymbol{y}_k = \boldsymbol{g}(\boldsymbol{u}_k)$ is generated experimentally, and $L \in \mathbb{R}^{pN\times mN}$ is a learning operator that is designed based on the system dynamics. The choice

$$L = \gamma(\boldsymbol{g}'(\boldsymbol{u}_k))^{-1} \tag{9}$$

where γ is a positive scalar, corresponds to applying the Newton method to iteratively minimise the cost $J_i(\boldsymbol{u}) = \|\boldsymbol{r}_i - \boldsymbol{g}(\boldsymbol{u})\|^2$. It was first introduced in the context of ILC by Lin et al. (2006) which demonstrated desirable properties including zero convergence error and a quadratic convergence rate. Alternatives were proposed in Freeman (2014) comprising

$$L = \gamma(\boldsymbol{g}'(\boldsymbol{u}_k))^\top, \tag{10}$$

$$L = \left(I + (\boldsymbol{g}'(\boldsymbol{u}_k))^\top \gamma \boldsymbol{g}'(\boldsymbol{u}_k)\right)^{-1} (\boldsymbol{g}'(\boldsymbol{u}_k))^\top \gamma. \tag{11}$$

The first is the result of applying gradient descent to the minimisation of $J_i(u)$, and the second 'norm optimal' form combines both Newton and gradient approaches. Further properties were derived in Huo et al. (2020). All three have been used in FES based stroke rehabilitation, with the gradient based update proving most robust to model uncertainty and most comfortable for patients (Freeman, 2016; Freeman et al., 2012) (see Table 1).

Computing L requires knowledge of the local system model about each operating point $\boldsymbol{u}_k$. This is given by

$$\boldsymbol{g}'(\boldsymbol{u}_k) := \left.\frac{\delta \boldsymbol{g}(\boldsymbol{u})}{\delta \boldsymbol{u}}\right|_{\boldsymbol{u}=\boldsymbol{u}_k} = \begin{bmatrix} \left.\frac{\delta g_1(\boldsymbol{u})}{\delta u_1}\right|_{\boldsymbol{u}=\boldsymbol{u}_k} & \dots & \left.\frac{\delta g_1(\boldsymbol{u})}{\delta u_m}\right|_{\boldsymbol{u}=\boldsymbol{u}_k} \\ \vdots & \ddots & \vdots \\ \left.\frac{\delta g_p(\boldsymbol{u})}{\delta u_1}\right|_{\boldsymbol{u}=\boldsymbol{u}_k} & \dots & \left.\frac{\delta g_p(\boldsymbol{u})}{\delta u_m}\right|_{\boldsymbol{u}=\boldsymbol{u}_k} \end{bmatrix} \tag{12}$$

$\in \mathbb{R}^{mN\times pN}$. In Lin et al. (2006), it was assumed that $\boldsymbol{g}(\boldsymbol{u}_k)$ was known, so $\boldsymbol{g}'(\boldsymbol{u}_k)$ was computed via simple linearisation. However, Freeman (2014), Ward et al. (2020), Yang et al. (2018) assumed $\boldsymbol{g}(\boldsymbol{u}_k)$ was unknown and must be identified through experiments. They proposed finding $\boldsymbol{g}'(\boldsymbol{u}_k)$ by solving identification problem

$$\boldsymbol{g}'(\boldsymbol{u}_k) := \arg\min_X J(X), \quad J(X) = \|\Delta \boldsymbol{y} - X\Delta \boldsymbol{u}\|^2 \tag{13}$$

where $X \in \mathbb{R}^{pN\times mN}$ with $(\Delta \boldsymbol{u}, \Delta \boldsymbol{y})$ chosen to sufficiently excite the system dynamics about $(\boldsymbol{u}_k, \boldsymbol{y}_k)$. To perform the identification, first $\Delta \boldsymbol{u}$ is chosen as a sufficiently exciting signal that is added to the operating point $\boldsymbol{u}_k$. The resulting input signal $\boldsymbol{u} = \boldsymbol{u}_k + \Delta \boldsymbol{u}$ is then applied experimentally and the generated output $\boldsymbol{y}$ is recorded. The component caused by $\Delta \boldsymbol{u}$ is determined as $\Delta \boldsymbol{y} = \boldsymbol{y} - \boldsymbol{y}_k$. Using (13), $\boldsymbol{g}'(\boldsymbol{u}_k)$ is then identified by fitting a linear model to $\{\Delta \boldsymbol{u}, \Delta \boldsymbol{y}\}$. The overall procedure is summarised in Algorithm 1. Here an outside loop has been added to track each reference from set $\mathcal{R}$, with the inner learning process starting from the same initial input $\boldsymbol{u}_0$ for each $\boldsymbol{r}_i \in \mathcal{R}$.

Algorithm 1 Standard ILC for multiple references

Require: Reference $\boldsymbol{r}_i \in \mathcal{R}$, accuracy margin δ
  for $i = 1 : n$ **do**
    Set $k = 0$. Select starting input, $\boldsymbol{u}_0$, for reference $\boldsymbol{r}_i$
    while $\left|J_i(\boldsymbol{u}_k) - J_i(\boldsymbol{u}^*)\right| < \delta$ **do**
      Apply $\boldsymbol{u}_k$ experimentally, record $\boldsymbol{y}_k = \boldsymbol{g}(\boldsymbol{u}_k)$.
      Identify $\boldsymbol{g}'(\boldsymbol{u}_k)$ by applying input $\boldsymbol{u} = \boldsymbol{u}_k + \Delta \boldsymbol{u}$ (where $\Delta \boldsymbol{u}$ is a small excitation signal), recording output $\boldsymbol{y} = \boldsymbol{y}_k + \Delta \boldsymbol{y}$, and fitting a linear model to $\{\Delta \boldsymbol{u}, \Delta \boldsymbol{y}\}$ by solving (13).
      Compute new ILC update using (8)
      $k = k + 1$
    end while
  end for

The above procedure was applied to FES arrays in Freeman (2014), Ward et al. (2020), Yang et al. (2018). Here $u(t)$ was the FES signal applied to $m = 24$ electrodes, and $y(t)$ was the $p = 12$ joint angles. The authors selected a value of $N = 1$ which corresponded to moving the hand from a resting position (at $t = 0$) to a functional gesture (at $t = 1$). This choice reduced the dimension of $\boldsymbol{g}'(\boldsymbol{u}_k)$ in (Eq. (12)) to an $m \times p$ matrix. To avoid patient discomfort, the excitation signal $\Delta \boldsymbol{u}$ was chosen as a slow ramp (of duration 8 s) applied to each electrode array element in turn. The identification procedure therefore required m experiments and lasted $8m = 192$ s. This approach was applied to track $n = 3$ gestures, and so a total of $3n(m + 1)$ experiments were needed. Fig. 1 shows these gestures which comprise open hand and pointing moments for switching lights and pushing buttons, and pinching movements for grasping and releasing objects. This was tested on two unimpaired subjects $P1$ and $P2$ who were instructed to provide no voluntary effort. Table 1 shows the percentage error calculated across all joints for each posture using $100 \times \frac{\|e_1\|}{\|e_0\|}$, where $\boldsymbol{e_0} = \boldsymbol{r}_i - \boldsymbol{y}_0$, with $\boldsymbol{y}_0$ the initial posture prior to stimulation. Each ILC trial reduced the error to approximately 30%, yielding results with a mean joint angle error of typically less than 5°.

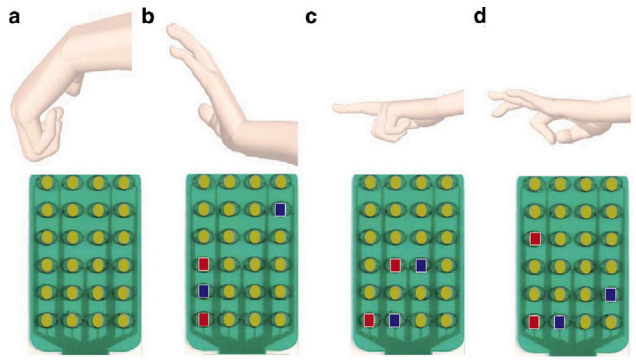

Fig. 1. Hand gestures and identified array elements (left hand view): (a) Starting, (b) Open hand, (c) Pointing, and (d) Pinch gestures (Freeman, 2014).

Table 1
Results for 3 iterations of each task in Freeman (2014), Ward et al. (2020), Yang et al. (2018).

		Pointing	Pinching	Open
$100\times\frac{\|e_1\|}{\|e_0\|}$	P1	29.72	24.48	19.08
	P2	28.66	35.31	22.16
$100\times\frac{\|e_2\|}{\|e_0\|}$	P1	11.18	12.62	14.36
	P2	13.61	14.98	13.01
$100\times\frac{\|e_3\|}{\|e_0\|}$	P1	3.58	4.37	4.67
	P2	1.45	3.89	3.45

3.1. Convergence results

Clearly, standard ILC methods incur substantial test data and time. To better quantify these requirements, this section will derive the relationship between the number of tests and the resulting accuracy (i.e. the parameters in (6)). Due to its suitability for rehabilitation, focus will be on update (10). However, currently no convergence conditions exist in ILC for (10), so they are derived next.

Theorem 1. *Suppose function $g(u)$ is differentiable and that error norm $J_i(u) := \|r_i - g(u)\|^2$ has a Lipschitz continuous gradient with constant $M > 0$. Then Algorithm 1 using ILC update law (8) with (10) yields an error norm sequence $\{\|e_k\|^2\}_{k=0,1,\ldots}$ that converges to a local minimum provided the learning gain is chosen to satisfy*

$$0 < \gamma < 4/M. \tag{14}$$

If $J_i(u)$ is also convex, this is a global minimum.

Proof. Since $\nabla J_i = J_i'(u_k)$ is Lipschitz continuous, it follows that $\nabla^2 J_i = J_i''(u_k) \preceq MI$ or equivalently $J_i''(u_k) - MI$ is a negative semidefinite matrix. Using this fact, a quadratic expansion of J_i around $J_i(u_k)$ is

$$\begin{aligned} J_i(u_{k+1}) \le\ & J_i(u_k) + (J_i'(u_k))^\top (u_{k+1} - u_k) \\ & + \frac{1}{2}\nabla^2 J_i(u_k)\|u_{k+1} - u_k\|^2 \qquad (15) \\ \le\ & J_i(u_k) + (J_i'(u_k))^\top (u_{k+1} - u_k) \\ & + \|u_{k+1} - u_k\|^2 M/2 \qquad (16) \end{aligned}$$

Then substitute $J_i'(u_k) = -2(g'(u_k))(r_i - g(u_k)) = -2(u_{k+1} - u_k)/\gamma$ into (16) to give

$$\begin{aligned} J_i(u_{k+1}) &\le J_i(u_k) - (2(u_{k+1} - u_k)/\gamma)^\top (u_{k+1} - u_k) \\ &\quad + \|u_{k+1} - u_k\|^2 M/2 \\ &= J_i(u_k) - (2/\gamma - M/2)\|u_{k+1} - u_k\|^2 \end{aligned} \tag{17}$$

Since (14) holds, $(2/\gamma - M/2) > 0$. It follows that the sequence $\{J_i(u_k)\}$ is non-increasing and converges since $J_i(u_k) \ge 0, J_i(u_{k+1}) \le J_i(u_k)$.

Denote $J_i^\infty := \lim_{k\to\infty} J_i(u_k)$ and taking the limit of both sides of (17) gives

$$\begin{aligned} J_i^\infty &= \lim_{k\to\infty} J_i(u_{k+1}) \\ &\le \lim_{k\to\infty} (J_i(u_k) - (2/\gamma - M/2)\|u_{k+1} - u_k\|^2) \\ &= J_i^\infty - (2/\gamma - M/2)\lim_{k\to\infty}\|u_{k+1} - u_k\|^2, \end{aligned} \tag{18}$$

which implies $\lim_{k\to\infty}\|u_{k+1} - u_k\|^2 = 0$. This combines with (10) to yield

$$\begin{aligned} \lim_{k\to\infty} -\gamma J_i'(u_k) &= 2\lim_{k\to\infty}\gamma(g'(u_k))^\top (r_i - g(u_k)) \\ &= \lim_{k\to\infty}(u_{k+1} - u_k) = 0. \end{aligned} \tag{19}$$

If J_i is also convex, then for any u,

$$J_i(u) \ge J_i(u_k) + (J_i'(u_k))^\top (u - u_k).$$

Taking the limit of the both sides gives

$$J_i(u) \ge J_i^\infty + \lim_{k\to\infty} 0^\top (u - u_k) = J_i^\infty$$

so that $J_i^\infty = \min_u J_i(u)$. □

Theorem 1 confirms that update (10) satisfies the ILC requirements of Definition 1, under mild assumptions which match those in Lin et al. (2006) and hold for numerous practical systems (e.g. those expressed by differentiable functions with a bounded derivative). It is now possible to bound the number of ILC trials required to track the entire set of n references, $\mathcal{R}$, as follows.

Theorem 2. *Suppose $J_i(u)$ is convex and ILC update law (8) with (10) is applied to track all references in the set $\mathcal{R}$ under the conditions of Theorem 1. An upper bound on the total number of iterations required to meet the accuracy conditions (6), (7) is*

$$k_\delta \le \sum_{i=1}^{n} \frac{\|u_0 - u_i^*\|^2}{2\gamma\delta}. \tag{20}$$

Proof. If J_i is convex, it follows that

$$J_i(u^*) \ge J_i(u) + J_i'(u)^\top (u^* - u) \tag{21}$$

$$J_i(u) \le J_i(u^*) + J_i'(u)^\top (u - u^*) \tag{22}$$

Substituting this into (17) and setting $\gamma = \frac{2}{M}$ yields

$$\begin{aligned} J_i(u_{k+1}) &\le J_i(u^*) + J_i'(u_k)^\top (u_k - u^*) - \frac{1}{\gamma}\|u_{k+1} - u_k\|^2 \\ J_i(u_{k+1}) - J_i(u^*) &\le J_i'(u_k)^\top (u_k - u^*) - \frac{1}{\gamma}\|u_{k+1} - u_k\|^2 \\ &\le \frac{1}{2\gamma}\big(2\gamma J_i'(u_k)^\top (u_k - u^*) - 2\|u_{k+1} - u_k\|^2 \\ &\quad - \|u_k - u^*\|^2 + \|u_k - u^*\|^2\big) \end{aligned} \tag{23}$$

Now note that

$$\begin{aligned} &(u_k - u^* - \gamma J_i'(u_k))^\top (u_k - u^* - \gamma J_i'(u_k)) \\ &= \|u_{k+1} - u^*\|^2 \\ &= \|u_k - u^*\|^2 - 2\gamma J_i'(u_k)^\top (u_k - u^*) \\ &\quad + \gamma^2 J_i'(u_k)^\top J_i'(u_k) \end{aligned} \tag{24}$$

so

$$\begin{aligned} J_i(u_{k+1}) - J_i(u^*) &\le \frac{1}{2\gamma}\Big(\|u_k - u^*\|^2 - \|u_{k+1} - u^*\|^2 \\ &\quad - 2\|u_{k+1} - u_k\|^2 + \gamma^2 J_i'(u_k)^\top J_i'(u_k)\Big) \\ &= \frac{1}{2\gamma}\Big(\|u_k - u^*\|^2 - \|u_{k+1} - u^*\|^2\Big) \end{aligned} \tag{25}$$

Summing over iterations yields

$$\sum_{j=0}^{k}\big(J_i(u_{j+1}) - J_i(u^*)\big)$$

$$\leq \sum_{j=0}^{k} \frac{1}{2\gamma}\left(\|\boldsymbol{u}_j - \boldsymbol{u}^*\|^2 - \|\boldsymbol{u}_{j+1} - \boldsymbol{u}^*\|^2\right)$$
$$= \frac{1}{2\gamma}\|\boldsymbol{u}^* - \boldsymbol{u}_0\|^2 - \gamma^{-1}\|\boldsymbol{u}_{k+1} - \boldsymbol{u}^*\|^2$$
$$\leq \frac{1}{2\gamma}\|\boldsymbol{u}^* - \boldsymbol{u}_0\|^2 \tag{26}$$

Since $J_i(u_0) \geq J_i(u_1) \geq \cdots \geq J_i(u_{k+1})$ by (17), then

$$\sum_{i=1}^{n} J_i(\boldsymbol{u}_{k+1}) - J_i(\boldsymbol{u}^*) \leq \sum_{i=1}^{n} \frac{1}{2\gamma(k+1)}\|\boldsymbol{u}_0 - \boldsymbol{u}_i^*\|^2$$
$$\leq \sum_{i=1}^{n} \frac{\|\boldsymbol{u}_0 - \boldsymbol{u}_i^*\|^2}{2\gamma\delta} \quad \square \tag{27}$$

Theorem 2 confirms the prohibitive time duration of current ILC approaches for FES arrays, since Algorithm 1 may take $\sum_{i=1}^{n} \frac{\|\boldsymbol{u}_0 - \boldsymbol{u}_i^*\|^2}{2\gamma\delta}$ iterations to track all references and δ is likely to be small.

4. Parameterised function ILC

The last section showed that standard ILC (Algorithm 1) requires many trials, each including a lengthy identification experiment to generate $\boldsymbol{g}'(\boldsymbol{u}_k)$. Since Algorithm 1 generates substantial data as it is applied to n references, a natural idea is to use these data to reduce the number of identification tests needed. This can be done by introducing a parameterised functional form of $\boldsymbol{g}(\boldsymbol{u})$ which replaces the identification of $\boldsymbol{g}(\boldsymbol{u}_k)$ within each update. Using parameter $\boldsymbol{\theta} \in \mathbb{R}^v$, this approximation is defined as

$$\bar{\boldsymbol{g}}(\boldsymbol{u}, \boldsymbol{\theta}) : (\mathbb{R}^{mN} \times \mathbb{R}^v) \to \mathbb{R}^{pN}. \tag{28}$$

Suppose a set of experimental input–output data is available, denoted $\{\boldsymbol{u}_i, \boldsymbol{y}_i\}_{i=1,2,\ldots}$. This set may have been generated by applying ILC to track previous references and it may also include data produced by applying ILC to track the current reference. Then $\boldsymbol{\theta}$ can be found by solving the standard identification problem of minimising the fitting error, i.e.

$$\hat{\boldsymbol{\theta}} = \min_{\boldsymbol{\theta}} \sum_i \|\boldsymbol{y}_i - \bar{\boldsymbol{g}}(\boldsymbol{u}_i, \boldsymbol{\theta})\|^2. \tag{29}$$

This approach is most effective if the parameter space is minimised. Hence the set up used in Freeman (2014) could be adopted in which $N = 1$ is taken, together with a sufficiently large sample time. This corresponds to moving the hand from a fixed starting position (at $t = 0$) to a desired reference position (at $t = 1$). The resulting $\boldsymbol{g}(\boldsymbol{u}) : \mathbb{R}^m \to \mathbb{R}^p$ then has a relatively small dimension. An example with $m = 2$, $p = 1$ is shown in Fig. 2. This shows a two input, one output system $\boldsymbol{y} = \boldsymbol{g}(\boldsymbol{u})$, which data points $\{\boldsymbol{u}_k, \boldsymbol{y}_k\}$ generated by applying Algorithm 1. Selecting $\bar{\boldsymbol{g}}(\boldsymbol{u}, \boldsymbol{\theta})$ as a piecewise linear mapping and computing $\hat{\boldsymbol{\theta}}$ using (Eq. (29)) gives the fitted forms shown in Fig. 2.

If the form $\bar{\boldsymbol{g}}(\boldsymbol{u}, \boldsymbol{\theta})$ is sufficiently accurate, it can be used in (8) to eliminate the identification step in Algorithm 1. The next result quantifies the necessary accuracy for convergence to minimal error occur. Although any of the learning operator choices (9)–(11) can be used, analysis will focus on the gradient form (10) since it has proven most suitable for rehabilitation. Note that the notation $\bar{\boldsymbol{g}}'(\boldsymbol{u}, \boldsymbol{\theta}) := \frac{\partial \bar{\boldsymbol{g}}(\boldsymbol{u}, \boldsymbol{\theta})}{\partial \boldsymbol{u}}$ is used to denote differentiation with respect to the first argument. Similarly the derivative of $\bar{J}_i(\boldsymbol{u}, \boldsymbol{\theta}) := \|\boldsymbol{r}_i - \bar{\boldsymbol{g}}(\boldsymbol{u}, \boldsymbol{\theta})\|^2$ is denoted $\bar{J}_i'(\boldsymbol{u}, \boldsymbol{\theta}) := \frac{\partial \bar{J}_i(\boldsymbol{u}, \boldsymbol{\theta})}{\partial \boldsymbol{u}}$ (see Figs. 2 and 3).

Theorem 3. *Let function $\boldsymbol{g}(\boldsymbol{u})$ be differentiable, and its parameterised approximation be denoted $\bar{\boldsymbol{g}}(\boldsymbol{u}, \boldsymbol{\theta})$. Let $J_i(\boldsymbol{u})$ satisfy the conditions of Theorem 1. Suppose the parameterised model satisfies*

$$\boldsymbol{g}'(\boldsymbol{u})^\top \bar{\boldsymbol{g}}'(\boldsymbol{u}, \boldsymbol{\theta}) \succ 0 \tag{30}$$

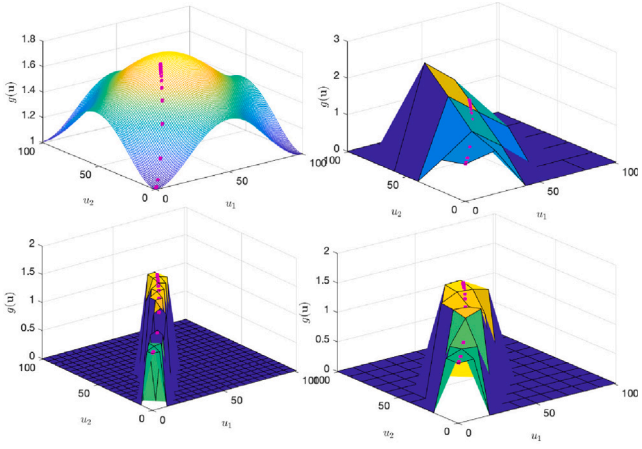

Fig. 2. Top left: mapping $\boldsymbol{y} = \boldsymbol{g}(\boldsymbol{u})$ with 2 inputs showing sequence of ILC points $\{\boldsymbol{u}_k, \boldsymbol{y}_k\}$. Other plots: Functions $\bar{\boldsymbol{g}}(\boldsymbol{u}, \boldsymbol{\theta})$ that are fitted to these data points using three different resolutions.

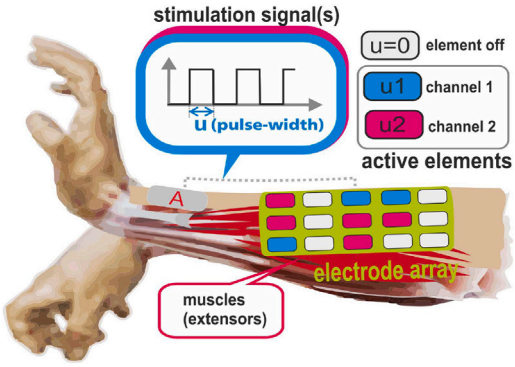

Fig. 3. FES array stimulation of wrist extensors using 2 FES input channels.

then the parameterised ILC gradient update

$$\boldsymbol{u}_{k+1} = \boldsymbol{u}_k + \gamma_k(\bar{\boldsymbol{g}}'(\boldsymbol{u}_k, \boldsymbol{\theta}))^\top(\boldsymbol{r}_i - \boldsymbol{y}_k) \tag{31}$$

with scalar gain

$$0 < \gamma_k < \frac{2\boldsymbol{e}_k^\top \boldsymbol{g}'(\boldsymbol{u}_k)(\bar{\boldsymbol{g}}'(\boldsymbol{u}_k, \boldsymbol{\theta}))^\top \boldsymbol{e}_k}{L\|\bar{J}_i'(\boldsymbol{u}_k, \boldsymbol{\theta})\|^2}. \tag{32}$$

guarantees convergence to the minimum error norm. If $J_i(\boldsymbol{u})$ is convex, this is the global minimum error norm.

Proof. Lipschitz continuity guarantees that

$$J_i(\boldsymbol{u}_{k+1}) \leq J_i(\boldsymbol{u}_k) + J_i'(\boldsymbol{u}_k)^\top(\boldsymbol{u}_{k+1} - \boldsymbol{u}_k) + \|\boldsymbol{u}_{k+1} - \boldsymbol{u}_k\|^2 \frac{L}{2}$$

Substitute $\bar{J}_i'(\boldsymbol{u}_k, \boldsymbol{\theta}) := -2\bar{\boldsymbol{g}}'(\boldsymbol{u}_k, \boldsymbol{\theta})^\top(\boldsymbol{r}_i - \boldsymbol{g}(\boldsymbol{u}_k))$ in the parameterised function ILC method to give

$$\boldsymbol{u}_{k+1} = \boldsymbol{u}_k + 2\gamma(\bar{\boldsymbol{g}}'(\boldsymbol{u}_k, \boldsymbol{\theta}))^\top(\boldsymbol{r}_i - \boldsymbol{g}(\boldsymbol{u}_k)) \tag{33}$$

so that

$$J_i(\boldsymbol{u}_{k+1}) \leq J_i(\boldsymbol{u}_k) + J_i'(\boldsymbol{u}_k)^\top(\boldsymbol{u}_k - \gamma\bar{J}_i'(\boldsymbol{u}_k, \boldsymbol{\theta}) - \boldsymbol{u}_k) + \|\boldsymbol{u}_k - \gamma\bar{J}_i'(\boldsymbol{u}_k, \boldsymbol{\theta}) - \boldsymbol{u}_k\|^2 L/2$$
$$= J_i(\boldsymbol{u}_k) - J_i'(\boldsymbol{u}_k)^\top \gamma\bar{J}_i'(\boldsymbol{u}_k, \boldsymbol{\theta}) + \|\gamma\bar{J}_i'(\boldsymbol{u}_k, \boldsymbol{\theta})\|^2 L/2$$
$$= J_i(\boldsymbol{u}_k) - \gamma J_i'(\boldsymbol{u}_k)^\top \bar{J}_i'(\boldsymbol{u}_k, \boldsymbol{\theta}) + \gamma^2\|\bar{J}_i'(\boldsymbol{u}_k, \boldsymbol{\theta})\|^2 L/2.$$

The term $J_i'(\boldsymbol{u}_k)^\top \bar{J}_i'(\boldsymbol{u}_k, \boldsymbol{\theta})$

$$= 4(\boldsymbol{r}_i - \boldsymbol{g}(\boldsymbol{u}_k))^\top \boldsymbol{g}'(\boldsymbol{u}_k)(\bar{\boldsymbol{g}}'(\boldsymbol{u}_k, \boldsymbol{\theta}))^\top(\boldsymbol{r}_i - \boldsymbol{g}(\boldsymbol{u}_k)) \tag{34}$$

is positive if assumption (30) holds, i.e.

$$\boldsymbol{g}'(\boldsymbol{u}_k)\bar{\boldsymbol{g}}'(\boldsymbol{u}_k,\boldsymbol{\theta})^\top \succ 0, \qquad \forall \boldsymbol{u}_k \neq \boldsymbol{u}^*. \tag{35}$$

Next denote $a_k := J_i'(\boldsymbol{u}_k)^\top \bar{J}_i'(\boldsymbol{u}_k,\boldsymbol{\theta})$ and select

$$0 < \gamma < \frac{2a_k}{L\|\bar{J}_i'(\boldsymbol{u}_k,\boldsymbol{\theta})\|^2} \tag{36}$$

so that the previous inequality becomes

$$\begin{aligned} J_i(\boldsymbol{u}_{k+1}) &\leq J_i(\boldsymbol{u}_k) - \gamma\Big(J_i'(\boldsymbol{u}_k)^\top \bar{J}_i'(\boldsymbol{u}_k,\boldsymbol{\theta}) - \gamma\|\bar{J}_i'(\boldsymbol{u}_k,\boldsymbol{\theta})\|^2\frac{L}{2}\Big) \\ &< J_i(\boldsymbol{u}_k) \end{aligned} \tag{37}$$

Suppose the selection $\gamma = \dfrac{a_k}{L\|\bar{J}_i'(\boldsymbol{u}_k,\boldsymbol{\theta})\|^2}$, is made, then

$$J_i(\boldsymbol{u}_{k+1}) < J_i(\boldsymbol{u}_k) - \gamma\big(a_k - a_k/2\big) = J_i(\boldsymbol{u}_k) - \gamma\frac{a_k}{2}. \tag{38}$$

Since a_k will always be positive unless $\boldsymbol{r}_i - \boldsymbol{g}(\boldsymbol{u}_k) = 0$, this inequality implies that the objective function value strictly decreases with each trial of gradient ILC until it reaches the optimal value $J_i(\boldsymbol{u}_k) = J_i(\boldsymbol{u}^*) = 0$. □

Theorem 3 provides a simple condition on the parameterised form $\bar{\boldsymbol{g}}(\boldsymbol{u}_k,\boldsymbol{\theta})$ which allows it to replace the true system $\boldsymbol{g}(\boldsymbol{u}_k)$, thus completely removing the need for any identification tests on trial k. Using Theorem 3, Algorithm 1 is replaced with Algorithm 2 to reduce the need for identification tests. This includes a test to establish whether sufficient condition (35) holds.

Algorithm 2 Parameterised function ILC

Require: Reference set $\mathcal{R}$, accuracy margin δ
for $i = 1 : n$ **do**
Set $k = 0$. Select an optimal starting input, $\boldsymbol{u}_0$, for reference $\boldsymbol{r}_i$ as

$$\boldsymbol{u}_0 := \min_{\boldsymbol{u}} \|\boldsymbol{r}_i - \bar{\boldsymbol{g}}(\boldsymbol{u},\hat{\boldsymbol{\theta}})\|^2 \tag{39}$$

while $|J_i(\boldsymbol{u}_k) - J_i(\boldsymbol{u}^*)| < \delta$ **do**
Apply $\boldsymbol{u}_k$ experimentally, record $\boldsymbol{y}_k = \boldsymbol{g}(\boldsymbol{u}_k)$.
Fit $\hat{\boldsymbol{\theta}}$ to all previous experimental data $\{\boldsymbol{u}_i, \boldsymbol{y}_i\}$ (e.g. generated from applying ILC to previous references, as well as previous ILC trials of the current reference) by solving

$$\hat{\boldsymbol{\theta}} := \min_{\boldsymbol{\theta}} \sum_i \|\boldsymbol{y}_i - \bar{\boldsymbol{g}}(\boldsymbol{u}_i,\boldsymbol{\theta})\|^2 \tag{40}$$

if $\boldsymbol{g}'(\boldsymbol{u}_k)^\top \bar{\boldsymbol{g}}'(\boldsymbol{u}_k,\hat{\boldsymbol{\theta}}) \succ 0$ holds **then**
Use the model to compute new ILC update using (31)
else
Identify $\boldsymbol{g}'(\boldsymbol{u}_k)$ by applying sufficiently exciting input $\boldsymbol{u}$ and solving (13).
Compute new ILC update using (8)
end if
$k = k + 1$
end while
end for

Note that selecting a sufficiently small fixed γ can always satisfy (32) without needing any knowledge of J_i. The term $\boldsymbol{g}'(\boldsymbol{u})^\top \bar{\boldsymbol{g}}'(\boldsymbol{u},\boldsymbol{\theta}) \succ 0$ is only required to hold for a convex set containing $\boldsymbol{u}_k$ and $\boldsymbol{u}_{k+1}$. Although $\boldsymbol{g}(\boldsymbol{u})$ is not known, the condition still has practical use since it instructs the designer to add more granularity to the model in locations where its gradient may deviate from that of the true system. The likely deviation can be assessed from previous data points, and the condition can always be guaranteed by adding more data points to the model in regions where $\boldsymbol{g}'(\boldsymbol{u})^\top$ is uncertain. The next Lemmas illustrate this, and also demonstrate advantages in using piece-wise linear forms for the model $\bar{\boldsymbol{g}}(\boldsymbol{u},\boldsymbol{\theta})$.

Lemma 1. *If $\bar{\boldsymbol{g}}(\boldsymbol{u},\boldsymbol{\theta})$ has the common linear-in-parameter form $G(\boldsymbol{u})\boldsymbol{\theta}$, then Eq. 40 becomes*

$$\hat{\boldsymbol{\theta}} := \min_{\boldsymbol{\theta}} \left\| \begin{bmatrix} \boldsymbol{y}_1 \\ \vdots \\ \boldsymbol{y}_n \end{bmatrix} - \begin{bmatrix} G(\boldsymbol{u}_1) \\ \vdots \\ G(\boldsymbol{u}_n) \end{bmatrix} \boldsymbol{\theta} \right\|^2 \tag{41}$$

with solution

$$\hat{\boldsymbol{\theta}} = \begin{bmatrix} G(\boldsymbol{u}_1) \\ \vdots \\ G(\boldsymbol{u}_n) \end{bmatrix}^\dagger \begin{bmatrix} \boldsymbol{y}_1 \\ \vdots \\ \boldsymbol{y}_n \end{bmatrix} \tag{42}$$

where $(\cdot)^\dagger$ denotes the generalised inverse. It can also be efficiently computed by the lower dimensional recursive form (see, e.g. Dahleh, Dahleh, and Verghese (2004))

$$\begin{aligned} \hat{\boldsymbol{\theta}}_{j+1} &= \hat{\boldsymbol{\theta}}_j + P_{j+1}G(\boldsymbol{u}_{j+1})^\top\big(\boldsymbol{y}_{j+1} - G(\boldsymbol{u}_{j+1})\hat{\boldsymbol{\theta}}_j\big), \\ P_{j+1} &= P_j - P_jG(\boldsymbol{u}_{j+1})^\top\big(I + G(\boldsymbol{u}_{j+1})P_jG(\boldsymbol{u}_{j+1})^\top\big)^{-1}\cdot \\ &\qquad G(\boldsymbol{u}_{j+1})P_j \end{aligned}$$

with initial condition $P_0 = I$, $j = 0, 1, \ldots, n-1$, $\hat{\boldsymbol{\theta}}_0 = 0$ and the solution $\hat{\boldsymbol{\theta}} = \hat{\boldsymbol{\theta}}_n$.

After finishing any experiment, the current solution $\hat{\boldsymbol{\theta}} = \hat{\boldsymbol{\theta}}_j$ is then updated, using the new input and output data $\{\boldsymbol{u}_{j+1}, \boldsymbol{y}_{j+1}\}$ to give the new solution $\hat{\boldsymbol{\theta}} = \hat{\boldsymbol{\theta}}_{j+1}$.

Lemma 2. *Let $\bar{\boldsymbol{g}}(\boldsymbol{u},\boldsymbol{\theta})$ take a piecewise linear form. Then (30) always holds providing the piecewise resolution is sufficiently fine and is fitted using sufficient data points. More pragmatically, if data points exist in all the segments neighbouring the one containing $\boldsymbol{u}_k$, then (35) holds, and Algorithm 2 will ultimately converge to a vertex of the segment containing solution $\boldsymbol{u}^*$.*

Proof. Given piecewise resolution $\Delta\boldsymbol{u}$, for any set $\{\boldsymbol{u}_i\}$

$$\lim_{\Delta\boldsymbol{u}\to 0} \min_{\boldsymbol{\theta}} \sum_i \|\boldsymbol{y}_i - \bar{\boldsymbol{g}}(\boldsymbol{u}_i,\boldsymbol{\theta})\|^2 = 0 \tag{43}$$

where $\boldsymbol{y}_i = \boldsymbol{g}(\boldsymbol{u}_i)$. Let $\cup_{\boldsymbol{u}_i} = \mathrm{dom}(\boldsymbol{g})$, then define

$$\boldsymbol{\theta}^* := \min_{\boldsymbol{\theta}} \sum_i \|\boldsymbol{y}_i - \bar{\boldsymbol{g}}(\boldsymbol{u}_i,\boldsymbol{\theta})\|^2 \tag{44}$$

it follows that $\lim_{\Delta\boldsymbol{u}\to 0} \boldsymbol{g}(\boldsymbol{u}_i) = \bar{\boldsymbol{g}}(\boldsymbol{u}_i,\boldsymbol{\theta}^*)\ \forall\, i$, and

$$\lim_{\Delta\boldsymbol{u}\to 0} \boldsymbol{g}'(\boldsymbol{u})^\top \bar{\boldsymbol{g}}'(\boldsymbol{u},\boldsymbol{\theta}^*) = \boldsymbol{g}'(\boldsymbol{u})^\top \boldsymbol{g}'(\boldsymbol{u}) \succ 0. \tag{45}$$

The second statement of Lemma 2 follows since monotonicity is preserved by linear interpolation. Therefore, if there exists a data point $\boldsymbol{u}_i$ in each segment neighbouring the segment containing $\boldsymbol{u}_k$ then $\boldsymbol{g}'(\boldsymbol{u}_k)\bar{\boldsymbol{g}}'(\boldsymbol{u}_k,\boldsymbol{\theta})^\top \succ 0$ holds provided the segment is locally monotonic (i.e. it does not contain a minimum $\boldsymbol{u}^*$). Convergence to a vertex adjoining $\boldsymbol{u}^*$ is therefore guaranteed by the proof of Theorem 3. □

Lemma 2 makes it possible to precisely evaluate the 'if' statement within Algorithm 2 to determine whether an experimental identification step is needed. The reduction in ILC trials provided by the new approach can now be established.

Theorem 4. *Suppose $J_i(\boldsymbol{u})$ is convex and parameterised function ILC is applied to track all references in the set $\mathcal{R}$ under the conditions of Theorem 3. Then an upper bound on the total number of iterations required to meet the accuracy metrics (k_δ, δ) in (6), (7) is*

$$k_\delta \leq \sum_{i=1}^{n}\Big\{\frac{\|\boldsymbol{u}_0 - \boldsymbol{u}_i^*\|^2}{2\gamma\delta} + \frac{\gamma}{2k}\sum_{i=0}^{k}\big(\bar{J}_i'(\boldsymbol{u}_i,\boldsymbol{\theta}) - J_i'(\boldsymbol{u}_i)\big)^\top \bar{J}_i'(\boldsymbol{u}_i,\boldsymbol{\theta})\Big\} \tag{46}$$

Proof. Since J_i is convex, it is possible to write

$$J_i(\boldsymbol{u}^*) \geq J_i(\boldsymbol{u}) + J_i'(\boldsymbol{u})^\top(\boldsymbol{u}^* - \boldsymbol{u}) \tag{47}$$

$$J_i(\boldsymbol{u}) \leq J_i(\boldsymbol{u}^*) + J_i'(\boldsymbol{u})^\top(\boldsymbol{u} - \boldsymbol{u}^*). \tag{48}$$

Substituting this into (38) yields

$$\begin{aligned}
J_i(\boldsymbol{u}_{k+1}) &\leq J_i(\boldsymbol{u}^*) + J_i'(\boldsymbol{u}_k)^\top(\boldsymbol{u}_k - \boldsymbol{u}^*) - \gamma a_k/2 \\
J_i(\boldsymbol{u}_{k+1}) - J_i(\boldsymbol{u}^*) &\leq J_i'(\boldsymbol{u}_k)^\top(\boldsymbol{u}_k - \boldsymbol{u}^*) - \gamma a_k/2 \\
J_i(\boldsymbol{u}_{k+1}) - J_i(\boldsymbol{u}^*) &\leq \frac{1}{2\gamma}\Big(2\gamma J_i'(\boldsymbol{u}_k)^\top(\boldsymbol{u}_k - \boldsymbol{u}^*) - \gamma^2 a_k \\
&\qquad - \|\boldsymbol{u}_k - \boldsymbol{u}^*\|^2 + \|\boldsymbol{u}_k - \boldsymbol{u}^*\|^2\Big)
\end{aligned} \tag{49}$$

Now note that

$$\begin{aligned}
&(\boldsymbol{u}_k - \boldsymbol{u}^* - \gamma \bar{J}_i'(\boldsymbol{u}_k, \boldsymbol{\theta}))^\top(\boldsymbol{u}_k - \boldsymbol{u}^* - \gamma \bar{J}_i'(\boldsymbol{u}_k, \boldsymbol{\theta})) \\
&= \|\boldsymbol{u}_{k+1} - \boldsymbol{u}^*\|^2 \\
&= \|\boldsymbol{u}_k - \boldsymbol{u}^*\|^2 - 2\gamma \bar{J}_i'(\boldsymbol{u}_k, \boldsymbol{\theta})^\top(\boldsymbol{u}_k - \boldsymbol{u}^*) \\
&\qquad + \gamma^2 \bar{J}_i'(\boldsymbol{u}_k, \boldsymbol{\theta})^\top \bar{J}_i'(\boldsymbol{u}_k, \boldsymbol{\theta})
\end{aligned}$$

so that

$$\begin{aligned}
J_i(\boldsymbol{u}_{k+1}) - J_i(\boldsymbol{u}^*) \leq \frac{1}{2\gamma}\Big(&\|\boldsymbol{u}_k - \boldsymbol{u}^*\|^2 - \|\boldsymbol{u}_{k+1} - \boldsymbol{u}^*\|^2 \\
&- \gamma^2\big(J_i'(\boldsymbol{u}_k) - \bar{J}_i'(\boldsymbol{u}_k, \boldsymbol{\theta})\big)^\top \bar{J}_i'(\boldsymbol{u}_k, \boldsymbol{\theta})\Big).
\end{aligned} \tag{50}$$

Summing over iterations produces

$$\begin{aligned}
&\sum_{i=0}^{k}\big(J_i(\boldsymbol{u}_{j+1}) - J_i(\boldsymbol{u}^*)\big) \\
&\leq \sum_{i=0}^{k}\frac{1}{2\gamma}\Big(\|\boldsymbol{u}_k - \boldsymbol{u}^*\|^2 - \|\boldsymbol{u}_{k+1} - \boldsymbol{u}^*\|^2 - \gamma^2\big(J_i'(\boldsymbol{u}_k) \\
&\qquad - \bar{J}_i'(\boldsymbol{u}_k, \boldsymbol{\theta})\big)^\top \bar{J}_i'(\boldsymbol{u}_k, \boldsymbol{\theta})\Big) \\
&\leq \frac{1}{2\gamma}\|\boldsymbol{u}_0 - \boldsymbol{u}^*\|^2 + \frac{\gamma}{2}\sum_{i=0}^{k}\big(\bar{J}_i'(\boldsymbol{u}_j, \boldsymbol{\theta}) - J_i'(\boldsymbol{u}_j)\big)^\top \bar{J}_i'(\boldsymbol{u}_i, \boldsymbol{\theta})
\end{aligned}$$

since J_i decreases on every iteration, it can be concluded

$$\begin{aligned}
J_i(\boldsymbol{u}_{k+1}) - J_i(\boldsymbol{u}^*) &\leq \frac{1}{k}\sum_{i=0}^{k}\big(J_i(\boldsymbol{u}_{k+1}) - J_i(\boldsymbol{u}^*)\big) \\
&\leq \frac{\|\boldsymbol{u}_0 - \boldsymbol{u}^*\|^2}{2\gamma k} + \frac{\gamma}{2k}\sum_{i=0}^{k}\big(\bar{J}_i'(\boldsymbol{u}_i, \boldsymbol{\theta}) - J_i'(\boldsymbol{u}_i)\big)^\top \bar{J}_i'(\boldsymbol{u}_i, \boldsymbol{\theta}). \quad \square
\end{aligned} \tag{51}$$

The last term in (46) reduces as $\bar{\boldsymbol{g}}(\boldsymbol{u}, \boldsymbol{\theta})$ more closely approximates the true system $\boldsymbol{g}(\boldsymbol{u})$. Theorem 4 therefore quantifies how the number of trials required for convergence depends on the accuracy of the model. Since model fitting improves as more experimental data are generated, it follows that new references are tracked progressively faster.

5. Numerical results

The approach is now evaluated on an FES array based motion control problem. The model is based on Theodorou, Todorov, and Valero-Cuevas (2011) and comprises a 3-link representation of the wrist and hand, including radius, metacarpal and phalangeal bones. The FES array elements are chosen to stimulate Flexor Digitorum Profundus and Extensor Communis muscles (u_1, u_2 respectively). The resultant force is transmitted via a longitudinally symmetric tendon rhombus network (including 5 active and 3 passive tendons) which actuates the wrist and metacarpal–phalangeal joints (y_1, y_2 respectively, in degrees). This $m = 2$, $p = 2$ system accurately models the response to FES, and the clinical aim is to achieve functional gestures such as 'open hand', 'pointing' or 'pinching' (Freeman, 2014). A set of $n = 4$ references is chosen to provide the variety required during an FES training session, given by $\boldsymbol{r}_1 = [10, 50]^\top$, $\boldsymbol{r}_2 = [70, 70]^\top$, $\boldsymbol{r}_3 = [20, 10]^\top$ and $\boldsymbol{r}_4 = [30, 50]^\top$.

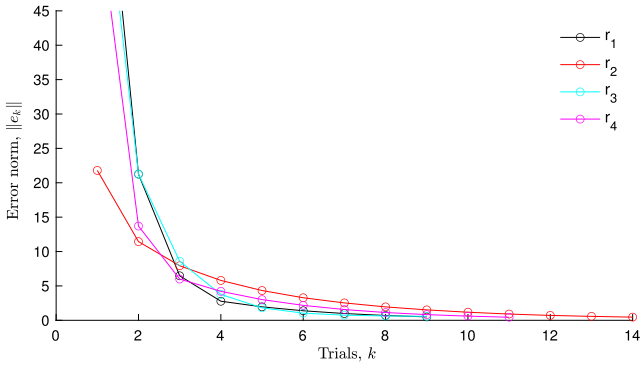

Fig. 4. Convergence of tracking error norm using standard ILC.

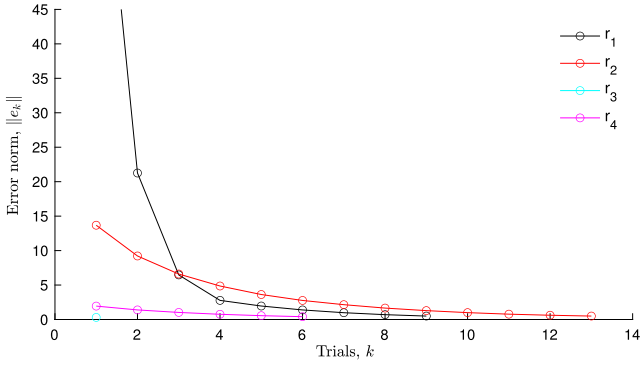

Fig. 5. Convergence of tracking error norm using parameterised function ILC with $\bar{\boldsymbol{g}}(\boldsymbol{u}_k, \boldsymbol{\theta})$ a medium resolution piecewise linear form.

5.1. Standard gradient ILC

First standard gradient ILC is applied using Algorithm 1 and a stopping criterion of $\delta = 0.05$ and initial input $\boldsymbol{u}_0 = [0, 0]^\top$. The error norm results are shown in Fig. 4. In total 43 ILC trials are required, each requiring 3 separate tests to perform. If applied experimentally, this equates to 129 tests in total. This is clearly too many for a typical clinical therapy session.

5.2. Parameterised function gradient ILC

Parameterised function ILC is next applied using Algorithm 2 and the same stopping criterion. Here $\bar{\boldsymbol{g}}(\boldsymbol{u}, \boldsymbol{\theta})$ is chosen as a piecewise linear functional form. Three choices of resolution are used in order investigate the compromise between accuracy and extrapolation potential (termed fine, medium and coarse).

The error norm results are shown in Fig. 5 for the medium resolution. Here a total of 29 ILC trials are required, however, only 9 of these require identification of a new model, with the remainder using parameterised model update (31) to generate the next update step. This means only 47 experimental tests would be needed in practice to track all references. To illustrate how this is achieved, $\bar{\boldsymbol{g}}(\boldsymbol{u}, \hat{\boldsymbol{\theta}})$ is shown in Fig. 6 immediately after completing $\boldsymbol{r}_2$ tracking. For the fine resolution case 12 ILC trials are required to track all references, however, only 9 of these require identification of a new model. This means 30 experimental tests would be needed in practice. For the coarse resolution, 32 ILC trials are required to track all references, however, again only 9 of these require identification of a new model. This means only 50 experimental tests would be needed in practice.

Overall, parameterised function ILC reduces the total number of ILC trials required for convergence from 43 to 12. In addition, the total number of experimental tests is reduced from 129 to 30, now making them clinically feasible.

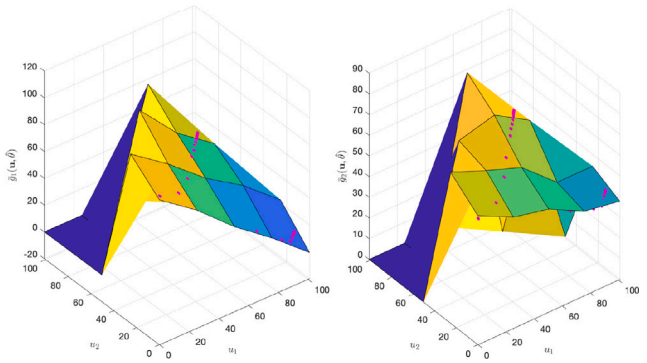

Fig. 6. Plots of $y_1 = \bar{g}_1(u, \hat{\theta})$ and $y_2 = \bar{g}_2(u, \hat{\theta})$ with all ILC points $\{u_k, y_k\}$ after completing r_2. .

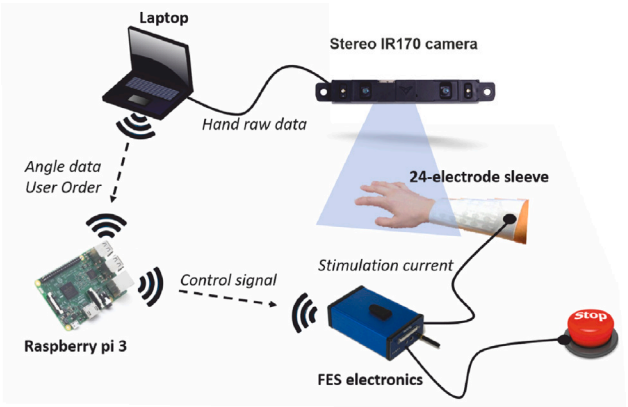

Fig. 7. Upper limb stroke rehabilitation hardware.

6. Experimental results

The hardware used consists of a tracking sensor, user interface software running on a laptop, a control unit, a 24 channel FES electrode array sleeve and FES electronics. The components are shown in Fig. 7. The sensor (Stereo IR 170 camera, UltraLeap) is a next-generation optical hand tracking module with a $170 \times 170°$ field of view, which collects the positional data of the hand and wrist, and is then processed by the user interface to generate angle data. This is sent to the control unit (Raspberry Pi 4) via wireless transmission, which runs the real-time controller (at 40 Hz). The controller computes the voltage pulse train applied to each element of the 24 channel electrode array. Here, the frequency and amplitude of each pulse train are fixed, and the pulse width of each pulse train is the controlled variable (0–100 μs). The sensor provides 12 joint angles, however only those corresponding to wrist flexion/extension and the index finger metacarpal–phalangeal joint flexion/extension are used. This matches the set-up of Section 5.

The simulation tests are now repeated experimentally in a study with six unimpaired participants (University of Southampton Ethics No. 72,855). These participants will be denoted P1, P2, P3, P4, P5, P6 and their details are shown in Table 2.

The experimental setup is shown in Fig. 8. The electrode array was first positioned on the forearm of the participant's dominant arm. Two stimulation sites were selected from the array, to correspond with activating the Flexor Digitorum Profundus and Extensor Communis muscles. Then a $100\mu s$ FES signal was applied to each of the two channels in turn. While stimulated, the voltage amplitude was slowly increased until a comfortable limit was reached. The pulsewidth was then reset to $0\mu s$ and the amplitude was then fixed for each channel in all remaining tests.

Table 2
Participant demographic information.

No.	Age	Gender	Test arm
P1	45	M	right
P2	42	F	right
P3	44	F	right
P4	38	M	left
P5	32	M	right
P6	31	F	right

Fig. 8. Electrode array, stimulator and Stereo IR 170 camera.

Three reference gestures (see Fig. 1) were used: open hand (with wrist and index finger extended), pinch (with wrist extended and index finger flexed), and horizontal pointing (with wrist partially extended and index finger fully extended). These are denoted r_1, r_2 and r_3 respectively. The values for participant P1 are $r_1 = [-31.8, 20.9]^\top$, $r_2 = [-33.6, 39.6]^\top$ and $r_3 = [-22.0, 14.1]^\top$ with unit in degrees, and a positive value corresponding to flexion for each angle.

Following this, the standard ILC and parameterised function ILC algorithms introduced in Sections 3 and 4 were applied. During each test, the participant was instructed to apply no voluntary effort, and they were not shown the reference movement. Note that omitting voluntary effort in the controller design has been assumed in all clinical trials using ILC (Freeman, Exell, Meadmore, Hallewell, & Hughes, 2015). This is because patients are typically highly impaired with significant weakness and so their voluntary input is minimal starting rehabilitation. Instead, their voluntary effort is treated as an external disturbance. At the end of each trial, the participant's hand naturally moved back to the start position under the influence of gravity.

As in the previous ILC applications of Freeman (2014), Yang et al. (2018), $N = 1$ was selected and the stimulation inputs were smoothly applied to each array element using a ramp signal of three seconds duration. The resulting hand gesture was measured.

In the previous section, the stopping criteria $\left|J_i(u_k) - J_i(u^*)\right| < \delta$ was used. During experiments, the value $J_i(u^*)$ is not known, and so it is assumed that perfect tracking is possible, $J_i(u^*) = 0$. This corresponds to the stopping criteria $\left|J_i(u_k) - J_i(u^*)\right| = \|e_k\| < \delta$. A value of $\delta = 5$ was selected as it corresponds to accurate tracking (i.e. joint angle error less than 5 degrees) that is considered practically achievable. The minimum number of trials to achieve this criteria will be termed the 'total trials', however the experiments will still be continued for ten trials in order to determine whether the level of error is maintained.

6.1. Standard ILC

First, standard ILC was applied as described in Algorithm 1 of Section 3. Two system gains were used for all participants: $\gamma = 10$ and

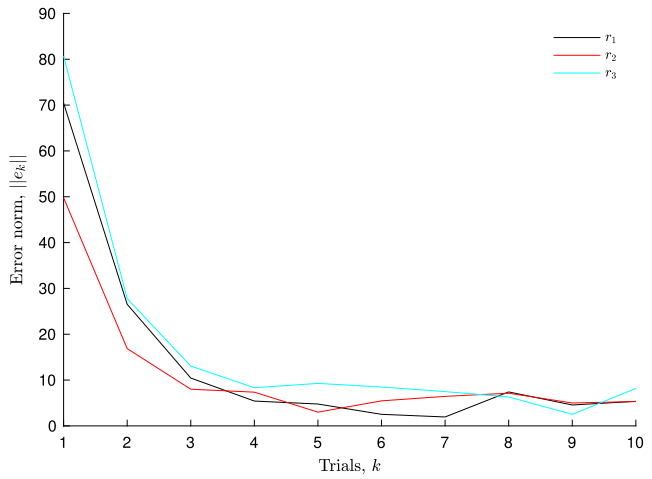

Fig. 9. Convergence of tracking error norm using standard ILC with $\gamma = 2$ for P1, (experimental results).

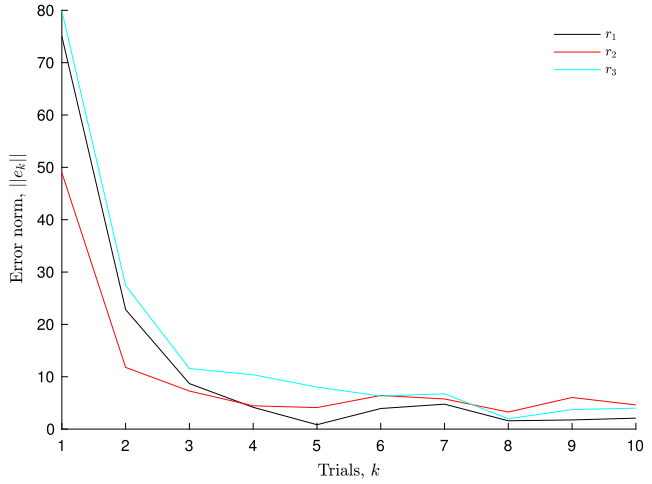

Fig. 10. Convergence of tracking error norm using standard ILC with $\gamma = 10$ for P1, (experimental results).

$\gamma = 2$. Results for participant P1 are shown in Fig. 9 for $\gamma = 2$. These confirm convergence to a low level of error for all three references.

Further convergence results for participant P1 are shown in Fig. 10 for $\gamma = 10$. These demonstrate faster convergence with high accuracy maintained over the ten trials.

For each reference, the number of trials required to meet the stopping criteria is listed in Table 3 for all participants. The total trial number is also shown. In all cases the increased ILC gain increases the convergence speed, however a large number of experiments is always required.

6.2. Parameterised function ILC

As in Section 4, Algorithm 2 was next applied with the same parameters as the standard ILC method. A vertex resolution of $25\mu s$ was used in the parameterised model form for all participants.

The error norm results for participant P1 using parameterised function ILC with $\gamma = 2$ are shown in Fig. 11. The convergence speed of parameterised function ILC is faster than standard ILC, since the later references start from a smaller initial error norm due to the use of the fitted model $\bar{\boldsymbol{g}}(\boldsymbol{u}, \hat{\boldsymbol{\theta}})$. A total of 19 ILC trials are required, however, only 6 of these require the identification of a new model, with the remainder using parameterised model update (31) to generate the next update

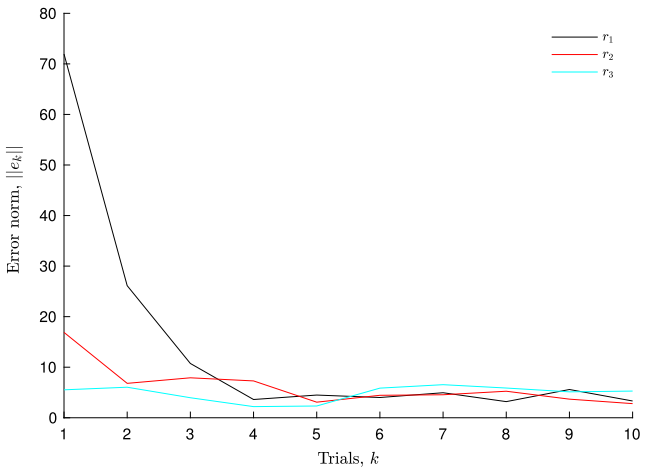

Fig. 11. Convergence of tracking error norm using parameterised function ILC with $\gamma = 2$ for P1, (experimental results).

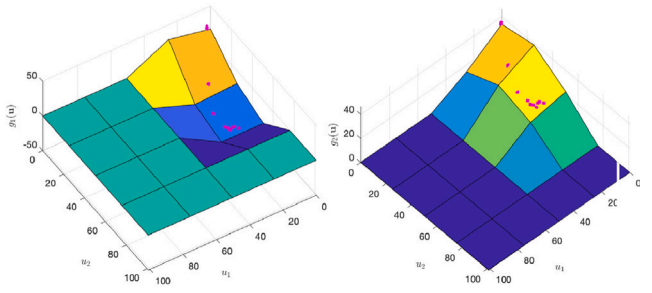

Fig. 12. Participant P1 results with $\gamma = 2$. Plots of $\boldsymbol{y}_1 = \bar{\boldsymbol{g}}_1(\boldsymbol{u}, \hat{\boldsymbol{\theta}})$ and $\boldsymbol{y}_2 = \bar{\boldsymbol{g}}_2(\boldsymbol{u}, \hat{\boldsymbol{\theta}})$ with all ILC points $\{\boldsymbol{u}_k, \boldsymbol{y}_k\}$ after completing $\boldsymbol{r}_1$, (experimental results).

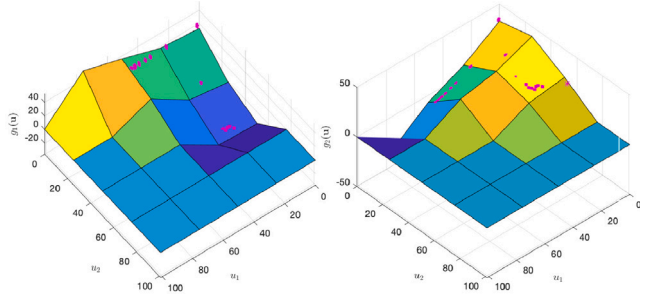

Fig. 13. Participant P1 results with $\gamma = 2$. Plots of $\boldsymbol{y}_1 = \bar{\boldsymbol{g}}_1(\boldsymbol{u}, \hat{\boldsymbol{\theta}})$ and $\boldsymbol{y}_2 = \bar{\boldsymbol{g}}_2(\boldsymbol{u}, \hat{\boldsymbol{\theta}})$ with all ILC points $\{\boldsymbol{u}_k, \boldsymbol{y}_k\}$ after completing $\boldsymbol{r}_2$, (experimental results).

step. This led to only 31 experimental tests being needed to track all three references. This equates to $31/57 = 54.4\%$ of the experiments required by Standard ILC. To show how this was achieved, the fitted model $\bar{\boldsymbol{g}}(\boldsymbol{u}, \hat{\boldsymbol{\theta}})$ is shown in Fig. 12 immediately after completing tracking of $\boldsymbol{r}_1$.

Fig. 13 shows the mapping immediately after completing tracking of $\boldsymbol{r}_2$. Information from the model in Fig. 12 has enabled the second reference to be tracked more quickly than with standard ILC.

Results using $\gamma = 10$ are shown in Fig. 14 for participant P1. These show even faster convergence.

For each reference, the overall total trial number is listed in Table 4 for all participants. In all cases there is significant improvement in terms of a reduced number of experiments required to achieve the three gestures.

Table 3
Total trials required by Standard ILC for all participants.

Trials \ Test / Participant	γ	r_1	r_2	r_3	Overall Trials	Overall Experiments
P1	2	5	5	9	19	57
	10	4	4	8	16	48
P2	2	5	6	9	20	60
	10	6	7	6	19	57
P3	2	5	5	9	19	57
	10	4	4	6	14	42
P4	2	10	4	10	24	72
	10	7	3	5	15	45
P5	2	9	4	10	23	69
	10	4	4	10	18	54
P6	2	9	10	10	29	87
	10	7	4	10	21	63

Table 4
Total trials required by parameterised function ILC for all participants. Improvement denotes the fraction of experiments compared with standard ILC.

Trials \ Test / Participant	γ	r_1	r_2	r_3	Overall Trials	Overall Experiments	Improvement
P1	2	6	7	6	19	31	54.40%
	10	4	3	3	10	18	37.50%
P2	2	4	2	8	14	22	36.66%
	10	4	2	5	11	19	33.33%
P3	2	10	5	2	17	37	64.91%
	10	4	3	4	11	19	45.23%
P4	2	4	5	1	10	18	25.00%
	10	7	3	5	15	29	64.40%
P5	2	10	7	7	24	44	63.76%
	10	8	2	9	19	35	64.81 %
P6	2	7	1	9	17	31	35.63%
	10	3	3	4	10	16	25.39%

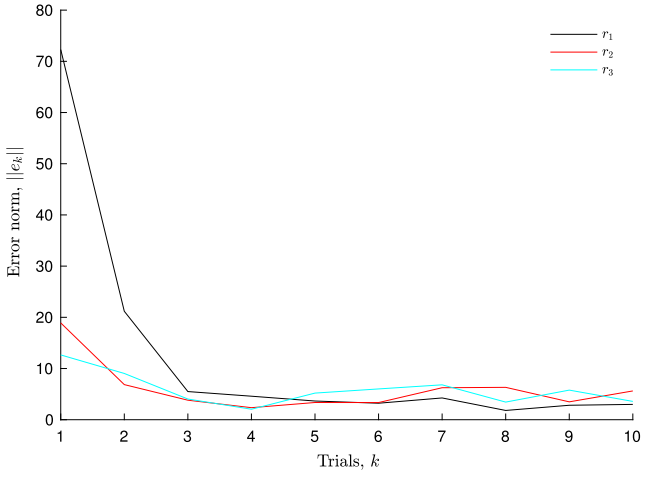

Fig. 14. Convergence of tracking error norm using parameterised function ILC with $\gamma = 10$ for P1, (experimental results).

7. Conclusions

A novel ILC approach is developed to reduce the experimental overhead required by existing model-free/data-driven approaches. It can be used for a general class of nonlinear systems, which includes the FES array based motion control problem. A parameterised model is fitted to all prior data and used to construct the next ILC update. Convergence conditions are derived to inform model design, minimising identification tests while preserving convergence. The framework is demonstrated on a key biomedical control problem, where the 129 experimental tests required using standard ILC are reduced to only 30. Experimental results with six participants confirm that accurate tracking is possible, both with standard ILC and parameterised function ILC. However, the latter reduces the number of experiments required to between 25% and 64.9% of those needed by the former.

Future work will focus on extending the convergence condition of Theorem 3 to hold for the Newton (9) and norm optimal (11) operators. Further work will also expand the system to include time-varying affects such as fatigue. Here, the application of parameterised function ILC will be unchanged, however, an additional parameter will be required to represent the level of fatigue together with an expanded model to embed the associated dynamics (e.g. 'low', 'medium' and 'high' fatigue).

The results and test procedures reported in this paper will also feed into an ethics application to gain the necessary authorisation prior to running clinical testing with stroke participants.

CRediT authorship contribution statement

Xiaoru Sun: Writing – review & editing, Writing – original draft. **Chris T. Freeman:** Supervision.

Declaration of competing interest

The authors declare that they have no known competing financial interests or personal relationships that could have appeared to influence the work reported in this paper.

References

Bijelić, G., Popović-Bijelić, A., Jorgovanović, N., Bojanić, D., & Popović, D. B. (2004). E actitrode: The new selective stimulation interface for functional movements in hemiplegic patients. *Serbian Journal of Electrical Engineering*, *1*(3), 21–28.

Crema, A., Malesevic, N., Furfaro, I., Raschella, F., Pedrocchi, A., & Micera, S. (2018). A wearable multi-site system for NMES-based hand function restoration. *IEEE Transactions on Neural Systems and Rehabilitation Engineering*, *26*(2), 428–440.

Dahleh, M., Dahleh, M. A., & Verghese, G. C. (2004). Lectures on dynamic systems and control. https://api.semanticscholar.org/CorpusID:1034511.

Feigin, V. L., Brainin, M., Norrving, B., Martins, S., Sacco, R. L., Hacke, W., et al. (2022). World Stroke Organization (WSO): Global stroke fact sheet 2022. *International Journal of Stroke*, *17*(1), 18–29.

Freeman, C. T. (2014). Electrode array-based electrical stimulation using ILC with restricted input subspace. *Control Engineering Practice*, *23*(2), 32–43.

Freeman, C. T. (2016). Control system design for electrical stimulation in upper limb rehabilitation. In *Springer international publishing*, (pp. 1–2).

Freeman, C. T., Exell, T., Meadmore, K., Hallewell, E., & Hughes, A.-M. (2015). Computational models of upper-limb motion during functional reaching tasks for application in FES-based stroke rehabilitation. *Biomedical Engineering*, *60*(3), 179–191.

Freeman, C. T., Rogers, E., Hughes, A.-M., Burridge, J. H., & Meadmore, K. L. (2012). Iterative learning control in health care: electrical stimulation and robotic-assisted upper-limb stroke rehabilitation. *IEEE Control Systems Magazine*, *32*(1), 18–43.

Hankey, G. J. (2017). Stroke. *The Lancet*, *389*(10069), 641–654.

Heller, B. W., Clarke, A. J., Good, T. R., Healey, T. J., Nair, S., & Pratt, E. J. (2013). Automated setup of functional electrical stimulation for drop foot using a novel 64 channel prototype stimulator and electrode array: Results from a gait-lab based study. *Medical Engineering & Physics*, *35*(1), 74–81.

Hoffmann, U., Deinhofer, M., & Keller, T. (2012). Automatic determination of parameters formultipad functional electrical stimulation: Application to hand opening and closing. *IEEE Engineering in Medicine and Biology Society*, 1859–1863. http://dx.doi.org/10.1109/EMBC.2012.6346314.

Hughes, A.-M., Burridge, J. H., Demain, S. H., Ellis-Hill, C., Meagher, C., Tedesco-Triccas, L., et al. (2014). Translation of evidence-based assistive technologies into stroke rehabilitation: Users' perceptions of the barriers and opportunities. *BMC Health Services Research*, *14*(1), 1–12.

Huo, B., Freeman, C. T., & Liu, Y. (2020). Data-driven gradient-based point-to-point iterative learning control for non-linear systems. *Nonlinear Dynamics*, *102*(1), 269–283.

Imatz.-Ojanguren, E., Irigoyen, E., & Keller, T. (2016). Reinforcement learning for hand graspwith surface multi-field neuroprostheses. In *International joint conference* (pp. 313–322).

Imatz.-Ojanguren, E., Irigoyen, E., Valencia-Blanco, D., & Keller, T. (2016). Neuro-fuzzy models for hand movements induced by functional electrical stimulation in able-bodied and hemiplegic subjects. *Medical Engineering & Physics*, *38*(11), 1–9.

Keller, T., Hackl, B., Lawrence, M., & Kuhn, A. (2006). Identification and control of handgrasp using multi-channel TES. In *Annual conference of the international FES society* (pp. 29–31).

Lin, T., Owens, D. H., & Hatonen, J. J. (2006). Newton method based iterative learning control for discrete non-linear systems. *International Journal of Control*, *79*(10), 1263–1276.

Malešević, N. M., Maneski, L. Z. P., Ilić, V., Jorgovanović, N., Bijelić, G., Keller, T., et al. (2012). A multi-pad electrode based functional electrical stimulation system for restoration of grasp. *Journal of NeuroEngineering and Rehabilitation*, *9*(1), 66.

Marchis, C. D., Monteiro, T. S., Simon-Martinez, C., Conforto, S., & Gharabaghi, A. (2016). Multi-contact functional electrical stimulation for hand opening: Electrophysiologically driven identification of the optimal stimulation site. *Journal of NeuroEngineering and Rehabilitation*, *13*(1), 22.

Molteni, F., Rossini, M., Gasperini, G., Davide, P., Krakow, K., & Nancy, I. (2018). A wearable hand neuroprosthesis for hand rehabilitation after stroke. In *INCR biosystems & biorobotics* (pp. 3–7).

O'Dwyer, S. B., O'Keeffe, D. T., Coote, S., & Lyons, G. M. (2006). An electrode configuration technique using an electrode matrix arrangement for FES-based upper arm rehabilitation systems. *Medical Engineering & Physics*, *28*, 166–176.

Pedrocchi, A., Ferrante, S., Ambrosini, E., Gandolla, M., Casellato, C., & Schauer, T. (2013). MUNDUS project: Multimodal neuroprosthesis for daily upper limb support. *Journal of NeuroEngineering and Rehabilitation*, *10*(1), 66.

Popović, D. B., & Popović, M. B. (2009). Automatic determination of the optimal shape of a surface electrode: selective stimulation. *Journal of Neuroscience Methods*, *178*(1), 174–181.

Popović-Maneski, L., Kostic, M., Bijelic, G., Keller, T., Mitrovic, S., Konstantinovic, L., et al. (2013). Multi-pad electrode for effective grasping: design. *IEEE Transactions on Neural Systems and Rehabilitation Engineering*, *21*(4), 648–654.

Popović-Maneski, L., Topalović, I., Jovičić, N., Dedijer, S., Konstantinović, L., & B.Popović, D. (2016). Stimulation map for control of functional grasp based on multi-channel EMG recordings. *Medical Engineering & Physics*, *38*(11), 1251–1259.

Rogers, E., Chu, B., Freeman, C. T., & Lewin, P. L. (2023). *Iterative learning control algorithms and experimental benchmarking*. John Wiley & Sons.

Salchow-Hömmen, C., Pedrocchi, A., & Keller, T. (2020). *Adaptive hand neuroprosthesis using inertial sensors for real-time motion tracking* (Ph.D. thesis), Technische Universität Berlin.

Schill, O., Rupp, R., Pylatiuk, C., Schulz, S., & Reischl, M. (2009). Automatic adaptation of a self-adhesive multi-electrode array for active wrist joint stabilization in tetraplegic SCI individuals. In *IEEE international conference science and technology for humanity* (pp. 708–713).

Sun, X., & Freeman, C. T. (2022). Parametrised function ILC with application to FES electrode arrays. In *American control conference* (pp. 4329–4334).

The Stroke Association (2023). National clinical guidelines for stroke for the United Kingdom and Ireland 2023. https://www.strokeguideline.org/contents/.

Theodorou, E., Todorov, E., & Valero-Cuevas, F. J. (2011). Neuromuscular stochastic optimal control of atendon driven index finger model. In *American control conference* (pp. 348–355).

Valtin, M., Kociemba, K., Behling, C., Kuberski, B., Becker, S., & Schauer, T. (2016). RehaMovePro: A versatile mobile stimulation system for transcutaneous FES applications. *European Journal of Translational Myology*, *26*(3), 203–208.

Velik, R., Malesevic, N., Maneski, L., Hoffmann, U., & Keller, T. (2011). INTFES: A multi-pad electrode system for selective transcutaneous electrical muscle stimulation. In *16th annual international functional electrical stimulation society conference* (pp. 8–11).

Ward, T., Grabham, N., Freeman, C. T., Wei, Y., Hughes, A.-M., Power, C., et al. (2020). Multichannel biphasic muscle stimulation system for post stroke rehabilitation. *Electronics*, *9*(7), 1156.

Yang, K., Meadmore, K., Freeman, C. T., Grabham, N., Hughes, A.-M., Wei, Y., et al. (2018). Development of user-friendly wearable electronic textiles for healthcare applications. *Sensors*, *18*(8), 2410.